*Journal of Sound and Vibration* (2003) **259**(4), 893–915
doi:10.1006/jsvi.2002.5128, available online at http://www.idealibrary.com on IDEAL®

# ESTIMATION OF 3D FIELD QUANTITIES AND ENERGY FLUX ASSOCIATED WITH ELASTIC WAVES IN A BAR

S. Widehammar

*TFM, Mid Sweden University, SE*-851 70 *Sundsvall, Sweden. E-mail: svante.widehammar@mh.se*

(*Received* 20 *September* 2001, *and in final form* 4 *March* 2002)

A method to estimate dispersion relations and warping associated with elastic wave propagation in a bar is presented. The method is based on Hamilton's principle. It is shown how the theoretical model together with strain measurements can be used to evaluate three dimensional (3D) field quantities like displacements and stresses at an arbitrary position in the bar, as well as energy flux through an arbitrary cross-section of the bar. It is also shown how redundant measurements can be used to increase the accuracy. The method is general and can be applied to any mode of wave propagation, isotropic or anisotropic linearly elastic material, and any cross-sectional geometry. Here, it is applied to longitudinal waves in a split Hopkinson pressure bar with linear elastic isotropic material behaviour and square cross-section. In particular, axial displacement, axial stress and energy flux are evaluated at a free end of the bar in order to test the method. The method is also used to estimate the Poisson ratio of the bar material, by measuring axial and transverse strains at the same axial position.

© 2002 Elsevier Science Ltd. All rights reserved.

## 1. INTRODUCTION

Longitudinal stress wave propagation in bars is often used in experimental work, like, e.g., in the split Hopkinson pressure bar (SHPB). If the waves carry significant energy at relatively high frequencies, dispersion must be taken into account. This is a standard procedure nowadays and has been used by, e.g., Follansbee and Frantz [1], Gong *et al.* [2] and Li and Lambros [3]. At high frequencies, the cross-section of the bar warps, and variables like stress and displacement vary over the cross-section. This effect has been studied experimentally [4] and with the aid of a finite element model [5] by Tyas and Watson, who showed that warping may not be negligible. For bars with circular cross-section, the warping and dispersion relations can be evaluated from the exact theoretical equations by Pochammer [6] and Chree [7] as done by Tyas and Watson. For arbitrary cross-sections, finite element methods have been used by, e.g., Hladky-Hennion [8], Volovoi *et al.* [9] and Taweel *et al.* [10].

Here, Hamilton's principle with matrix formulations similar to those used in the finite element method, has been employed but with co-ordinate functions valid over the whole cross-section. The resulting eigenvalue problem has been formulated to become real-valued. Similar formulations have been made previously for the finite element method by, e.g., Hladky-Hennion and Volovoi *et al.* A method to solve the eigenvalue problem by inverse iterations for a number of consecutive frequencies and a special mode of wave propagation is suggested.

It has been shown here how the theoretical model and experimental data can be combined to determine wave propagation in a bar. With the procedure used, dispersion

0022-460X/02/$35.00 © 2002 Elsevier Science Ltd. All rights reserved.

and warping are taken into account automatically. The theoretical model allows variables like stress, strain and displacement to be expressed as functions of time and position in the bar. An expression for the energy flux through a cross-section of the bar has also been formulated. Typically, the conditions at the end of the bar are of interest. The functions are Fourier series which makes the method very fast if a fast Fourier transform (FFT) technique is used.

It has been shown by, e.g., Lundberg and Henchoz [11], Zhao and Gary [12] and Bacon [13] how measurements of strains at two positions can be used to separate waves travelling in the two opposite directions through a bar. Park and Zhou [14] replaced one of the measurements by an end condition of the bar. Zhao and Gary as well as Bacon, pointed out that a problem arises when working in the frequency domain if the distance between the two measuring positions equals an integral multiple of half the wavelength. This condition is always approximately true for some frequency components. They solved the problem by also working in the time domain.

Here, a method has been used which employs three or more strain gauges in order to obtain redundant data. This method alleviates the problem with critical frequencies and allows one to work completely in the frequency domain. Also, it has been shown how redundant data can be obtained from only two measuring positions. This can be done when the waves travelling in the two directions are separated in time for at least one measuring position, as in the most common set-up for SHPB experiments. The method of using redundant data to get better accuracy in connection with wave propagation in bars has been used previously by Hillström *et al.* [15] in order to estimate the complex modulus of a viscoelastic bar.

The method to find dispersion relations and warping can be applied to bars with arbitrary cross-section, isotropic or anisotropic linearly elastic material and any mode of wave propagation, e.g., longitudinal, flexural or torsional. A general and detailed description of the formulation to be used was given in Widehammar *et al.* [16]. Here, this formulation has been summarized and further developed. The method to couple the theoretical model to experimental data, preferably using redundant measurements, can be used in a variety of applications. Examples are SHPB experiments [17], mechanical impedance gauges [18], force–penetration measurements in rock drilling [19] and dynamic measurements of frictional properties at an end of a bar [20].

Longitudinal waves in a bar with square cross-section has been considered as an example here. Cartesian co-ordinates and isotropic linearly elastic material have been used. Experiments which validate the method have been carried out. In particular, the displacements and stresses at a free bar end have been evaluated, as well as the energy flux through the bar end.

## 2. THEORETICAL BACKGROUND

In the absence of external forces, Hamilton's principle states that

$$\delta\left(\int_{t_1}^{t_2}(T-U)\,\mathrm{d}t\right)=0, \tag{1}$$

where $T$ is the kinetic energy, $U$ is the elastic strain energy and $t_1$ and $t_2$ are two arbitrary instants of time $t$. The kinetic energy is give by

$$T=\int\int\int_V\left(\frac{1}{2}\rho\dot{\mathbf{u}}^{\mathrm{T}}\dot{\mathbf{u}}\right)\mathrm{d}V, \tag{2}$$

where $\rho$ is the mass density, $\mathbf{u} = [\mathbf{u}_x, \mathbf{u}_y, \mathbf{u}_z]^{\mathrm{T}}$ is the displacement vector, $V$ is the volume of the body, and an "overdot" denotes partial differentiation with respect to time $t$. Cartesian co-ordinates $x$, $y$ and $z$ are used. The elastic strain energy of the body is

$$U = \int\int\int_V \left(\frac{1}{2}\boldsymbol{\tau}^{\mathrm{T}}\boldsymbol{\varepsilon}\right) \mathrm{d}V, \tag{3}$$

where $\boldsymbol{\tau} = [\sigma_x, \sigma_y, \sigma_z, \tau_{xy}, \tau_{yz}, \tau_{zx}]^{\mathrm{T}}$ and $\boldsymbol{\varepsilon} = [\varepsilon_x, \ldots, \gamma_{zx}]^{\mathrm{T}}$ are vectors containing the components of stress and strain, respectively. For a linearly elastic and isotropic material, the generalized Hooke's law is given by

$$\boldsymbol{\tau} = E\mathbf{C}\boldsymbol{\varepsilon}, \tag{4}$$

where $E$ is Young's modulus and $\mathbf{C}$ is the symmetric matrix of normalized elastic constants. The vector of strain components $\boldsymbol{\varepsilon}$ and the displacement vector $\mathbf{u}$ are related through the kinematic relation

$$\boldsymbol{\varepsilon} = \boldsymbol{\nabla}\boldsymbol{u}, \tag{5}$$

where $\boldsymbol{\nabla}$ contains the partial differential operators $\partial/\partial x$, $\partial/\partial y$ and $\partial/\partial z$. For a study of wave propagation in a bar with its axis oriented in the $z$-direction, it is suitable to split the matrix $\boldsymbol{\nabla}$ into two parts, i.e.,

$$\boldsymbol{\nabla} = \boldsymbol{\nabla}_{xy} + \boldsymbol{\nabla}_z a \frac{\partial}{\partial z}, \tag{6}$$

where $\boldsymbol{\nabla}_{xy}$ contains partial differential operators $\partial/\partial x$ and $\partial/\partial y$ and $\boldsymbol{\nabla}_z$ is a constant matrix. The parameter $a$ is a reference length, such as the radius of a circular bar or half the side length of a bar with square cross-section. It is introduced in order to obtain the same physical dimension of $\boldsymbol{\nabla}_{xy}$ and $\boldsymbol{\nabla}_z$. An approximate displacement field associated with a propagating wave can be written

$$\mathbf{u} = \mathrm{Re}\{A\boldsymbol{\Phi}(x, y)\mathbf{d}\mathrm{e}^{\mathrm{i}(\omega t - kz)}\}, \tag{7}$$

where $A$ is a complex-valued amplitude, $\boldsymbol{\Phi}$ is a $(3 \times m)$ matrix containing given co-ordinate functions, $\mathbf{d}$ is a normalized vector of $m$ complex-valued constants, $\omega$ is the angular frequency and $k$ is the wavenumber. The amplitude $A$ has the physical dimension of length, while $\boldsymbol{\Phi}$ and $\mathbf{d}$ are dimensionless. Equations (2)–(7), inserted into Hamilton's principle (1), leads to the eigenvalue problem

$$\left(\mathbf{K}_0 + \mathrm{i}\frac{k}{k_0}(\mathbf{K}_1 - \mathbf{K}_1^{\mathrm{T}}) + \left(\frac{k}{k_0}\right)^2 \mathbf{K}_2 - \left(\frac{\omega}{\omega_0}\right)^2 \mathbf{M}\right)\mathbf{d} = \mathbf{0}, \tag{8}$$

where

$$k_0 = \frac{1}{a}, \qquad \omega_0 = \sqrt{\frac{E}{a^2\rho}} \tag{9}$$

are reference quantities and

$$\mathbf{K}_0 = \int\int_S (\boldsymbol{\nabla}_{xy}\boldsymbol{\Phi})^{\mathrm{T}}\mathbf{C}\boldsymbol{\nabla}_{xy}\boldsymbol{\Phi}\,\mathrm{d}S, \qquad \mathbf{K}_1 = \int\int_S \boldsymbol{\Phi}^{\mathrm{T}}\boldsymbol{\nabla}_z^{\mathrm{T}}\mathbf{C}\boldsymbol{\nabla}_{xy}\boldsymbol{\Phi}\,\mathrm{d}S, \tag{10, 11}$$

$$\mathbf{K}_2 = \int\int_S \boldsymbol{\Phi}^{\mathrm{T}}\boldsymbol{\nabla}_z^{\mathrm{T}}\mathbf{C}\boldsymbol{\nabla}_z\boldsymbol{\Phi}\,\mathrm{d}S, \tag{12}$$

and

$$\mathbf{M} = \frac{1}{a^2}\int\int_S \mathbf{\Phi}^{\mathrm{T}}\mathbf{\Phi}\,\mathrm{d}S \tag{13}$$

are dimensionless matrices. The quantity $S$ is the cross-sectional area of the bar. The details of derivation can be found in reference [16].

The eigenvalue to solve for is one of the quantities $k/k_0$ or $\omega/\omega_0$ with the other known. For a given angular frequency $\omega$, this is a quadratic eigenvalue problem with $2m$ solutions. The eigenvalue $k/k_0$ is generally complex-valued, but for modes corresponding to propagating waves, $k/k_0$ is real. Non-real wavenumbers correspond to end modes which decay with distance from the bar end, see e.g. reference [10]. Suppose that a solution $(k, \mathbf{d})$, where $k$ is positive and real, is found. This corresponds to a wave travelling in the positive $z$-direction. Then, by forming the complex conjugate of equation (8), one can show that $(-k, \mathbf{d}^*)$, where a "star" denotes complex conjugate, is also a solution to the eigenvalue problem. This second solution corresponds to a wave of the same mode which travels in the negative $z$-direction. The approximate displacement field for waves of one single mode which travels in both directions, can then be written as

$$\mathbf{u} = \mathrm{Re}\{A\mathbf{\Phi}\mathbf{d}\mathrm{e}^{\mathrm{i}(\omega t - kz)} + B\mathbf{\Phi}\mathbf{d}^*\mathrm{e}^{\mathrm{i}(\omega t + kz)}\}. \tag{14}$$

From here on, the notation "Re" for real part will be left out if there is no risk of confusion.

## 3. SOLVING THE EIGENVALUE PROBLEM

In an experimental test, the interest is normally focused on a particular propagating mode. The eigenvalue $k/k_0$ of the eigenvalue problem (8) is then real-valued, and it is well known from the literature that $u_x$ and $u_y$ are phase shifted $\pi/2$ from $u_z$, see e.g. Kolsky [21]. By dividing all matrices into submatrices, and rearranging the eigenvalue problem (8), one can transfer it to a real-valued problem with symmetric matrices, which has real eigenvectors for the propagating modes.

The known phase shift between $u_x$ and $u_y$ on one hand, and $u_z$ on the other hand, motivates one to divide the vector $\mathbf{u}$ and the right-hand side of equation (7) into

$$\mathbf{u} = \begin{bmatrix} \mathbf{u}^a \\ \mathbf{u}^b \end{bmatrix} = \begin{bmatrix} \mathbf{\Phi}^a & \mathbf{0} \\ \mathbf{0} & \mathbf{\Phi}^b \end{bmatrix} \begin{bmatrix} \mathbf{d}^a \\ \mathbf{d}^b \end{bmatrix} A\mathrm{e}^{\mathrm{i}(\omega t - kz)}, \tag{15}$$

where $\mathbf{u}^a = [u_x, u_y]^{\mathrm{T}}$, $\mathbf{u}^b = [u_z]$ (scalar), $\mathbf{\Phi}^a$ is a $(2 \times m_a)$ matrix and $\mathbf{\Phi}^b$ is a $(1 \times m_b)$ matrix. It should be noted that $\mathbf{\Phi}^a$ and $\mathbf{d}^a$ express the co-ordinate functions and degrees of freedom connected to displacements in the transverse directions, and $\mathbf{\Phi}^b$ and $\mathbf{d}^b$ are connected to axial displacements. Then, the vector of strain components $\boldsymbol{\varepsilon}$ can be split into

$$\boldsymbol{\varepsilon} = \begin{bmatrix} \boldsymbol{\varepsilon}^a \\ \boldsymbol{\varepsilon}^b \end{bmatrix}, \qquad \boldsymbol{\varepsilon}^a = \begin{bmatrix} \varepsilon_x \\ \varepsilon_y \\ \varepsilon_z \\ \gamma_{xy} \end{bmatrix}, \qquad \boldsymbol{\varepsilon}^b = \begin{bmatrix} \gamma_{yz} \\ \gamma_{zx} \end{bmatrix}, \tag{16}$$

the matrices $\boldsymbol{\nabla}_{xy}$ and $\boldsymbol{\nabla}_z$ into

$$\boldsymbol{\nabla}_{xy} = \begin{bmatrix} \boldsymbol{\nabla}_{xy}^a & \mathbf{0} \\ \mathbf{0} & \boldsymbol{\nabla}_{xy}^b \end{bmatrix}, \qquad \boldsymbol{\nabla}_{xy}^a = \begin{bmatrix} \dfrac{\partial}{\partial x} & 0 \\ 0 & \dfrac{\partial}{\partial y} \\ 0 & 0 \\ \dfrac{\partial}{\partial y} & \dfrac{\partial}{\partial x} \end{bmatrix}, \qquad \boldsymbol{\nabla}_{xy}^b = \begin{bmatrix} \dfrac{\partial}{\partial y} \\ \dfrac{\partial}{\partial x} \end{bmatrix} \tag{17}$$

and the matrix $\boldsymbol{\nabla}_z$ into

$$\boldsymbol{\nabla}_z = \begin{bmatrix} \mathbf{0} & \boldsymbol{\nabla}_z^b \\ \boldsymbol{\nabla}_z^a & \mathbf{0} \end{bmatrix}, \qquad \boldsymbol{\nabla}_z^a = \frac{1}{a}\begin{bmatrix} 0 & 1 \\ 1 & 0 \end{bmatrix}, \qquad \boldsymbol{\nabla}_z^b = \frac{1}{a}\begin{bmatrix} 0 \\ 0 \\ 1 \\ 0 \end{bmatrix}, \tag{18}$$

respectively. Similarly, the vector of stress components $\boldsymbol{\tau}$ can be split into

$$\boldsymbol{\tau} = \begin{bmatrix} \boldsymbol{\tau}^a \\ \boldsymbol{\tau}^b \end{bmatrix}, \qquad \boldsymbol{\tau}^a = \begin{bmatrix} \sigma_x \\ \sigma_y \\ \sigma_z \\ \tau_{xy} \end{bmatrix}, \qquad \boldsymbol{\tau}^b = \begin{bmatrix} \tau_{yz} \\ \tau_{zx} \end{bmatrix}, \tag{19}$$

and the normalized matrix of elastic constants into

$$\mathbf{C} = \begin{bmatrix} \mathbf{C}^a & \mathbf{0} \\ \mathbf{0} & \mathbf{C}^b \end{bmatrix}, \qquad \mathbf{C}^a = \begin{bmatrix} \alpha_1 & \alpha_2 & \alpha_2 & 0 \\ \alpha_2 & \alpha_1 & \alpha_2 & 0 \\ \alpha_2 & \alpha_2 & \alpha_1 & 0 \\ 0 & 0 & 0 & \alpha_3 \end{bmatrix}, \qquad \mathbf{C}^b = \begin{bmatrix} \alpha_3 & 0 \\ 0 & \alpha_3 \end{bmatrix} \tag{20}$$

with

$$\alpha_1 = \frac{1-\nu}{(1+\nu)(1-2\nu)}, \qquad \alpha_2 = \frac{\nu}{(1+\nu)(1-2\nu)}, \qquad \alpha_3 = \frac{1}{2(1+\nu)}, \tag{21}$$

where $\nu$ is the Poisson ratio.

The eigenvalue problem (8) can be expressed as

$$\mathbf{J}\left(\mathbf{K}_0 + \mathrm{i}\frac{k}{k_0}(\mathbf{K}_1 - \mathbf{K}_1^{\mathrm{T}}) + \left(\frac{k}{k_0}\right)^2 \mathbf{K}_2 - \left(\frac{\omega}{\omega_0}\right)^2 \mathbf{M}\right)\mathbf{J}^{-1}\mathbf{J}\mathbf{d} = \mathbf{0}, \tag{22}$$

where

$$\mathbf{J} = \begin{bmatrix} \mathbf{I} & \mathbf{0} \\ \mathbf{0} & \mathrm{i}\mathbf{I} \end{bmatrix}, \qquad \mathbf{J}^{-1} = \begin{bmatrix} \mathbf{I} & \mathbf{0} \\ \mathbf{0} & -\mathrm{i}\mathbf{I} \end{bmatrix} \tag{23}$$

and $\mathbf{I}$ is the unity matrix. Inserting the submatrices defined above, creating the vector $\tilde{\mathbf{d}} = \mathbf{J}\mathbf{d}$, multiplying $\mathbf{J}$ and $\mathbf{J}^{-1}$ into the parentheses and simplifying, one obtains

$$\left(\tilde{\mathbf{K}}_0 + \frac{k}{k_0}(\tilde{\mathbf{K}}_1 + \tilde{\mathbf{K}}_1^{\mathrm{T}}) + \left(\frac{k}{k_0}\right)^2 \tilde{\mathbf{K}}_2 - \left(\frac{\omega}{\omega_0}\right)^2 \tilde{\mathbf{M}}\right)\tilde{\mathbf{d}} = \mathbf{0}, \tag{24}$$

where

$$\tilde{\mathbf{K}}_0 = \iint_S \begin{bmatrix} (\boldsymbol{\nabla}_{xy}^a \boldsymbol{\Phi}^a)^{\mathrm{T}} \mathbf{C}^a \boldsymbol{\nabla}_{xy}^a \boldsymbol{\Phi}^a & \mathbf{0} \\ \mathbf{0} & (\boldsymbol{\nabla}_{xy}^b \boldsymbol{\Phi}^b)^{\mathrm{T}} \mathbf{C}^b \boldsymbol{\nabla}_{xy}^b \boldsymbol{\Phi}^b \end{bmatrix} \mathrm{d}S, \tag{25}$$

$$\tilde{\mathbf{K}}_1 = \iint_S \begin{bmatrix} \mathbf{0} & \boldsymbol{\Phi}^{a\mathrm{T}} \boldsymbol{\nabla}_z^{a\mathrm{T}} \mathbf{C}^b \boldsymbol{\nabla}_{xy}^b \boldsymbol{\Phi}^b \\ -\boldsymbol{\Phi}^{b\mathrm{T}} \boldsymbol{\nabla}_z^{b\mathrm{T}} \mathbf{C}^a \boldsymbol{\nabla}_{xy}^a \boldsymbol{\Phi}^a & \mathbf{0} \end{bmatrix} \mathrm{d}S, \tag{26}$$

$$\tilde{\mathbf{K}}_2 = \iint_S \begin{bmatrix} \boldsymbol{\Phi}^{a\mathrm{T}} \boldsymbol{\nabla}_z^{a\mathrm{T}} \mathbf{C}^b \boldsymbol{\nabla}_z^a \boldsymbol{\Phi}^a & \mathbf{0} \\ \mathbf{0} & \boldsymbol{\Phi}^{b\mathrm{T}} \boldsymbol{\nabla}_z^{b\mathrm{T}} \mathbf{C}^a \boldsymbol{\nabla}_z^b \boldsymbol{\Phi}^b \end{bmatrix} \mathrm{d}S, \tag{27}$$

$$\tilde{\mathbf{M}} = \frac{1}{a^2} \iint_S \begin{bmatrix} \boldsymbol{\Phi}^{a\mathrm{T}} \boldsymbol{\Phi}^a & \mathbf{0} \\ \mathbf{0} & \boldsymbol{\Phi}^{b\mathrm{T}} \boldsymbol{\Phi}^b \end{bmatrix} \mathrm{d}S \tag{28}$$

and

$$\tilde{\mathbf{d}} = \begin{bmatrix} \mathbf{d}^a \\ \mathrm{i}\mathbf{d}^b \end{bmatrix}. \tag{29}$$

The four matrices $\tilde{\mathbf{K}}_0$, $(\tilde{\mathbf{K}}_1 + \tilde{\mathbf{K}}_1^{\mathrm{T}})$, $\tilde{\mathbf{K}}_2$ and $\tilde{\mathbf{M}}$ are real and symmetric, and it can be shown that

$$\mathbf{K}_0 = \tilde{\mathbf{K}}_0, \qquad \mathbf{K}_2 = \tilde{\mathbf{K}}_2, \qquad \mathbf{M} = \tilde{\mathbf{M}} \tag{30}$$

and

$$\mathbf{K}_1 = \begin{bmatrix} \mathbf{I} & \mathbf{0} \\ \mathbf{0} & -\mathbf{I} \end{bmatrix} \tilde{\mathbf{K}}_1. \tag{31}$$

If $k/k_0$ is given, equation (24) is a generalized eigenvalue problem with real-valued symmetric matrices. Thus, the eigenvalues $(\omega/\omega_0)^2$ and eigenvectors $\tilde{\mathbf{d}}$ are real. If instead $\omega/\omega_0$ is given, the eigenvalues $k/k_0$ are generally complex-valued, but the propagating modes have real $k/k_0$ and real $\tilde{\mathbf{d}}$. The fact that $\tilde{\mathbf{d}}$ is real for propagating modes means that $\mathbf{d}^a$ is real-valued and $\mathbf{d}^b$ is imaginary, which leads to $\mathbf{d}^* = [\mathbf{d}^{a\mathrm{T}}, -\mathbf{d}^{b\mathrm{T}}]^{\mathrm{T}}$. Inserting the submatrices given above into equations (14), (5), (6) and (4) one obtains

$$\mathbf{u} = \begin{bmatrix} \mathbf{u}^a \\ \mathbf{u}^b \end{bmatrix} = \begin{bmatrix} \boldsymbol{\Phi}^a \mathbf{d}^a \\ \boldsymbol{\Phi}^b \mathbf{d}^b \end{bmatrix} A\mathrm{e}^{\mathrm{i}(\omega t - kz)} + \begin{bmatrix} \boldsymbol{\Phi}^a \mathbf{d}^a \\ -\boldsymbol{\Phi}^b \mathbf{d}^b \end{bmatrix} B\mathrm{e}^{\mathrm{i}(\omega t + kz)}, \tag{32}$$

$$\begin{aligned} \boldsymbol{\varepsilon} = \begin{bmatrix} \boldsymbol{\varepsilon}^a \\ \boldsymbol{\varepsilon}^b \end{bmatrix} = & \begin{bmatrix} \boldsymbol{\nabla}_{xy}^a \boldsymbol{\Phi}^a \mathbf{d}^a - \mathrm{i}ka \boldsymbol{\nabla}_z^b \boldsymbol{\Phi}^b \mathbf{d}^b \\ \boldsymbol{\nabla}_{xy}^b \boldsymbol{\Phi}^b \mathbf{d}^b - \mathrm{i}ka \boldsymbol{\nabla}_z^a \boldsymbol{\Phi}^a \mathbf{d}^a \end{bmatrix} A\mathrm{e}^{\mathrm{i}(\omega t - kz)} \\ & + \begin{bmatrix} \boldsymbol{\nabla}_{xy}^a \boldsymbol{\Phi}^a \mathbf{d}^a - \mathrm{i}ka \boldsymbol{\nabla}_z^b \boldsymbol{\Phi}^b \mathbf{d}^b \\ -\boldsymbol{\nabla}_{xy}^b \boldsymbol{\Phi}^b \mathbf{d}^b + \mathrm{i}ka \boldsymbol{\nabla}_z^a \boldsymbol{\Phi}^a \mathbf{d}^a \end{bmatrix} B\mathrm{e}^{\mathrm{i}(\omega t + kz)} \end{aligned} \tag{33}$$

and

$$\begin{aligned} \boldsymbol{\tau} = \begin{bmatrix} \boldsymbol{\tau}^a \\ \boldsymbol{\tau}^b \end{bmatrix} = & E \begin{bmatrix} \mathbf{C}^a \boldsymbol{\nabla}_{xy}^a \boldsymbol{\Phi}^a \mathbf{d}^a - \mathrm{i}ka \mathbf{C}^a \boldsymbol{\nabla}_z^b \boldsymbol{\Phi}^b \mathbf{d}^b \\ \mathbf{C}^b \boldsymbol{\nabla}_{xy}^b \boldsymbol{\Phi}^b \mathbf{d}^b - \mathrm{i}ka \mathbf{C}^b \boldsymbol{\nabla}_z^a \boldsymbol{\Phi}^a \mathbf{d}^a \end{bmatrix} A\mathrm{e}^{\mathrm{i}(\omega t - kz)} \\ & + E \begin{bmatrix} \mathbf{C}^a \boldsymbol{\nabla}_{xy}^a \boldsymbol{\Phi}^a \mathbf{d}^a - \mathrm{i}ka \mathbf{C}^a \boldsymbol{\nabla}_z^b \boldsymbol{\Phi}^b \mathbf{d}^b \\ -\mathbf{C}^b \boldsymbol{\nabla}_{xy}^b \boldsymbol{\Phi}^b \mathbf{d}^b + \mathrm{i}ka \mathbf{C}^b \boldsymbol{\nabla}_z^a \boldsymbol{\Phi}^a \mathbf{d}^a \end{bmatrix} B\mathrm{e}^{\mathrm{i}(\omega t + kz)}. \end{aligned} \tag{34}$$

It can be seen that $\mathbf{u}^a$, $\boldsymbol{\varepsilon}^a$ and $\boldsymbol{\tau}^a$ are in phase with each other, but phase-shifted $\pi/2$ relative to $\mathbf{u}^b$, $\boldsymbol{\varepsilon}^b$ and $\boldsymbol{\tau}^b$.

In this work, inverse iteration according to Ruhe [22] was used to solve the eigenvalue problem (24) for the desired mode of wave propagation at each angular frequency

$$\omega_j = (j-1)\Delta\omega, \quad j = 1, 2, \ldots. \tag{35}$$

The solution for $\omega = \omega_j$ was used as an initial guess for $\omega = \omega_{j+1}$. This method is very fast and gives a solution only for the mode of interest. Furthermore, the eigenvectors have the proper phase angle (i.e. zero) directly, which is not guaranteed using standard functions in mathematical toolboxes like, e.g., Matlab.

## 4. CONDITIONS IN A SHPB

In a SHPB, the first mode of longitudinal waves in the two directions is present. It will be assumed that the influence from other modes is negligible. The displacement field associated with waves in the bar can be transformed from the time domain into the frequency domain, and *vice versa*, using the discrete Fourier transform (DFT). A general expression for an approximate displacement field is

$$\begin{aligned}\mathbf{u} = {} & (u_0 + v_0 t)[0, 0, 1]^{\mathrm{T}} + \varepsilon_0[-\nu x, -\nu y, z]^{\mathrm{T}} \\ & + \sum_{p=2}^{M/2} (A_p \boldsymbol{\Phi}\mathbf{d}_p \mathrm{e}^{\mathrm{i}(\omega_p t - k_p z)} + B_p \boldsymbol{\Phi}\mathbf{d}_p^* \mathrm{e}^{\mathrm{i}(\omega_p t + k_p z)}),\end{aligned} \tag{36}$$

where $M$ is the number of samples in the DFT. The constant term in the DFT of the displacements is related to a constant strain $\varepsilon_0$ in the axial direction of the bar. This term does not represent waves and is separated from the sum for clarity. In addition, rigid-body motion in the axial direction can be present in the bar. The co-ordinate functions in $\boldsymbol{\Phi}$ are independent of $p$ and can be taken out of the sum, which gives

$$\mathbf{u} = (u_0 + v_0 t)\mathbf{r} + \varepsilon_0 \mathbf{e} + \boldsymbol{\Phi}\mathbf{w}, \tag{37}$$

where the vectors $\mathbf{r} = [0, 0, 1]^{\mathrm{T}}$ and $\mathbf{e} = [-\nu x, -\nu y, z]^{\mathrm{T}}$ represent rigid-body motion and a constant strain, respectively, while the vector

$$\mathbf{w}(z, t) = \sum_{p=2}^{M/2} (A_p \mathbf{d}_p \mathrm{e}^{-\mathrm{i}k_p z} + B_p \mathbf{d}_p^* \mathrm{e}^{\mathrm{i}k_p z})\, \mathrm{e}^{\mathrm{i}\omega_p z} \tag{38}$$

represents wave propagation. The expression for $\mathbf{w}$, i.e., the real part of the sum in equation (38), is best computed using an inverse DFT when the variables in the sum are known.

From equations (5), (6), (17), (18) and (37), one obtains

$$\boldsymbol{\varepsilon} = \varepsilon_0[-\nu, -\nu, 1, 0, 0, 0]^{\mathrm{T}} + \boldsymbol{\nabla}_{xy}\boldsymbol{\Phi}\mathbf{w} + \boldsymbol{\nabla}_z \boldsymbol{\Phi} a \mathbf{w}', \tag{39}$$

where

$$\mathbf{w}' = \sum_{p=2}^{M/2} (-A_p \mathbf{d}_p \mathrm{e}^{-\mathrm{i}k_p z} + B_p \mathbf{d}_p^* \mathrm{e}^{\mathrm{i}k_p z})\, \mathrm{i}k_p \mathrm{e}^{\mathrm{i}\omega_p t} \tag{40}$$

is the derivative of $\mathbf{w}$ with respect to $z$. From equations (4), (20), (21) and (39), the vector of stress components can be obtained as

$$\boldsymbol{\tau} = E\varepsilon_0[0,0,1,0,0,0]^{\mathrm{T}} + E\mathbf{C}\boldsymbol{\nabla}_{xy}\boldsymbol{\Phi}\mathbf{w} + E\mathbf{C}\boldsymbol{\nabla}_z\boldsymbol{\Phi}a\mathbf{w}'. \tag{41}$$

## 5. MEAN VALUES OVER A CROSS-SECTION

In experimental studies, interest is often devoted to conditions at a specific cross-section, e.g., at the end of the bar. From the previous sections, variables like $\mathbf{u}$ and $\boldsymbol{\tau}$ can be calculated as functions of time at an arbitrary position $(x, y, z)$ of the bar. Such detailed information over the cross-section is normally too ambitious because of the inaccuracy of measurements and the possible existence of end modes. Instead, it may be valuable to obtain a mean value of a variable over the cross-section. For the displacement components, the mean values are

$$\bar{\mathbf{u}}(z_c, t) = \frac{1}{S}\int\int_S \mathbf{u}(x, y, z_c, t)\,\mathrm{d}S, \tag{42}$$

where $z_c$ is the $z$-co-ordinate of the specified cross-section. Equation (37) gives

$$\bar{\mathbf{u}}(z_c, t) = (u_0 + v_0 t)\mathbf{r} + \varepsilon_0[0,0,z_c]^{\mathrm{T}} + \mathbf{F}\mathbf{w}(z_c, t), \tag{43}$$

where

$$\mathbf{F} = \frac{1}{S}\int\int_S \boldsymbol{\Phi}\,\mathrm{d}S. \tag{44}$$

The components $\bar{u}_x$ and $\bar{u}_y$ are zero in a SHPB.

The stress components in $\boldsymbol{\tau}$ are given by equation (41), and the mean values over the cross-section are

$$\bar{\boldsymbol{\tau}}(z_c, t) = E\varepsilon_0[0,0,1,0,0,0]^{\mathrm{T}} + E\mathbf{C}\mathbf{F}_{xy}\mathbf{w} + E\mathbf{C}\mathbf{F}_z a\mathbf{w}', \tag{45}$$

where

$$\mathbf{F}_{xy} = \frac{1}{S}\int\int_S (\boldsymbol{\nabla}_{xy}\boldsymbol{\Phi})\,\mathrm{d}S \tag{46}$$

and

$$\mathbf{F}_z = \frac{1}{S}\int\int_S (\boldsymbol{\nabla}_z\boldsymbol{\Phi})\,\mathrm{d}S \quad (= \boldsymbol{\nabla}_z\mathbf{F}). \tag{47}$$

## 6. ENERGY FLUX AT A CROSS-SECTION

The stress vector at a point of a cross-section of the bar, $\mathbf{t} = [\tau_{zx}, \tau_{yz}, \sigma_z]^{\mathrm{T}}$, can be expressed as

$$\mathbf{t} = a\boldsymbol{\nabla}_z^{\mathrm{T}}\boldsymbol{\tau}. \tag{48}$$

This result follows from the natural boundary conditions obtained with Hamilton's principle. Inserting equations (18) and (41) into equation (48), one obtains

$$\mathbf{t} = E\varepsilon_0[0,0,1]^{\mathrm{T}} + Ea\boldsymbol{\nabla}_z^{\mathrm{T}}\mathbf{C}\boldsymbol{\nabla}_{xy}\boldsymbol{\Phi}\mathbf{w} + Ea^2\boldsymbol{\nabla}_z^{\mathrm{T}}\mathbf{C}\boldsymbol{\nabla}_z\boldsymbol{\Phi}\mathbf{w}'. \tag{49}$$

The energy flux in positive $z$ direction through the cross-section is

$$P(z,t) = -\int\int_S \dot{\mathbf{u}}^{\mathrm{T}}\mathbf{t}\,\mathrm{d}S. \tag{50}$$

With use of equations (37) and (49), one obtains

$$\begin{aligned} P(z,t) = & -\int\int_S (v_0\mathbf{r}^{\mathrm{T}} + \dot{\mathbf{w}}^{\mathrm{T}}\boldsymbol{\Phi}^{\mathrm{T}}) \\ & \times (E\varepsilon_0[0,0,1]^{\mathrm{T}} + Ea\boldsymbol{\nabla}_z^{\mathrm{T}}\mathbf{C}\boldsymbol{\nabla}_{xy}\boldsymbol{\Phi}\mathbf{w} + Ea^2\boldsymbol{\nabla}_z^{\mathrm{T}}\mathbf{C}\boldsymbol{\nabla}_z\boldsymbol{\Phi}\mathbf{w}')\,\mathrm{d}S, \end{aligned} \tag{51}$$

where

$$\dot{\mathbf{w}} = \sum_{p=2}^{M/2}(A_p\mathbf{d}_p\mathrm{e}^{-\mathrm{i}k_pz} + B_p\mathbf{d}_p^*\mathrm{e}^{\mathrm{i}k_pz})\,\mathrm{i}\omega_p\mathrm{e}^{\mathrm{i}\omega_pt} \tag{52}$$

is the derivative of $\mathbf{w}$ with respect to time. Simplification gives

$$\begin{aligned} P(z,t) = & -E\int\int_S v_0\varepsilon_0 + v_0\mathbf{C}_3(\boldsymbol{\nabla}_{xy}\boldsymbol{\Phi}\mathbf{w} + a\boldsymbol{\nabla}_z\boldsymbol{\Phi}\mathbf{w}') \\ & + \varepsilon_0\dot{\mathbf{w}}^{\mathrm{T}}\boldsymbol{\Phi}_3^{\mathrm{T}} + a\dot{\mathbf{w}}^{\mathrm{T}}\boldsymbol{\Phi}^{\mathrm{T}}\boldsymbol{\nabla}_z^{\mathrm{T}}\mathbf{C}(\boldsymbol{\nabla}_{xy}\boldsymbol{\Phi}\mathbf{w} + a\boldsymbol{\nabla}_z\boldsymbol{\Phi}\mathbf{w}')\,\mathrm{d}S, \end{aligned} \tag{53}$$

where $\mathbf{C}_3$ and $\boldsymbol{\Phi}_3$ denote the third row of each matrix. Evaluating the integral, one obtains

$$\begin{aligned} P(z,t) = & -E(Sv_0\varepsilon_0 + Sv_0\mathbf{C}_3(\mathbf{F}_{xy}\mathbf{w} + a\mathbf{F}_z\mathbf{w}') \\ & + S\varepsilon_0\dot{\mathbf{w}}^{\mathrm{T}}\mathbf{F}_3^{\mathrm{T}} + a\dot{\mathbf{w}}^{\mathrm{T}}(\mathbf{K}_1\mathbf{w} + a\mathbf{K}_2\mathbf{w}')). \end{aligned} \tag{54}$$

## 7. EXPERIMENTAL CALIBRATION OF THE BAR

In the equations above, there are only four parameters which depend on the bar in the experimental set-up, i.e., $a$, $\rho$, $E$ and $v$. The first two are easy to determine, but if no reliable material data are available, it can be cumbersome to determine $E$ and $v$. A test specimen must be manufactured and a testing machine must be used. Another way to determine these parameters, directly from the bar in use, is as follows.

Young's modulus $E$ can be determined by measuring the time for the wave to travel a known distance. The phase velocity

$$c_0 = \sqrt{\frac{E}{\rho}} \tag{55}$$

for longitudinal waves with infinite wavelength is dominant, so measuring this velocity and knowing the density $\rho$ will give Young's modulus $E$.

A way to determine the Poisson ratio $v$, is to measure the strain in the axial and transverse directions at the same axial position. The vector of strain components $\boldsymbol{\varepsilon}^a = [\varepsilon_x, \varepsilon_y, \varepsilon_z, \gamma_{xy}]^{\mathrm{T}}$ in a SHPB is obtained by using equations (33) and (39) to obtain

$$\boldsymbol{\varepsilon}^a = \varepsilon_0[-v, -v, 1, 0]^{\mathrm{T}} + \sum_{p=2}^{M/2}\mathbf{q}_p(A_p\mathrm{e}^{-\mathrm{i}k_pz} + B_p\mathrm{e}^{\mathrm{i}k_pz})\,\mathrm{e}^{\mathrm{i}\omega_pt}, \tag{56}$$

where

$$\mathbf{q}_p = \boldsymbol{\nabla}_{xy}^a\boldsymbol{\Phi}^a\mathbf{d}_p^a - \mathrm{i}k_pa\boldsymbol{\nabla}_z^b\boldsymbol{\Phi}^b\mathbf{d}_p^b. \tag{57}$$

According to equation (56), the ratio of the axial to the transverse strain as a function of time is

$$\left(\frac{\varepsilon_z}{\varepsilon_y}\right)_{theoretical} = \frac{\varepsilon_0 + \mathbf{p}_z^{\mathrm{T}} \sum_{p=2}^{M/2} \mathbf{q}_p (A_p e^{-ik_p z} + B_p e^{ik_p z})\, e^{i\omega_p t}}{-\nu\varepsilon_0 + \mathbf{p}_y^{\mathrm{T}} \sum_{p=2}^{M/2} \mathbf{q}_p (A_p e^{-ik_p z} + B_p e^{ik_p z})\, e^{i\omega_p t}}, \tag{58}$$

where the vectors $\mathbf{p}_y^{\mathrm{T}} = [0, 1, 0, 0]$ and $\mathbf{p}_z^{\mathrm{T}} = [0, 0, 1, 0]$ are used to pick the right strain component. Note that the values of the co-ordinates $x$ and $y$ in the matrix $\mathbf{\Phi}$, included in $\mathbf{q}_p$, should correspond to the positions of the strain gauges.

From a measurement of the strain component $\varepsilon_\beta$, where $\beta$ is one of $x$, $y$ and $z$, at position $(x_j, y_j, z_j)$, one gets the discrete time signal

$$\varepsilon_\beta(x_j, y_j, z_j, t_q) = \varepsilon_j(t_1 + (q-1)\Delta t) = \varepsilon_{jq}, \quad q = 1, 2, \ldots, M, \tag{59}$$

where $\Delta t$ is the sampling interval. The corresponding DFT is

$$\hat{\varepsilon}_{jp} = \sum_{q=1}^{M} \varepsilon_{jq} e^{-i2\pi((q-1)(p-1)/M)}, \quad p = 1, \ldots, M. \tag{60}$$

The time signal can be viewed as the sum of trigonometric functions

$$\varepsilon_j(t) = C_{j1} + \sum_{p=2}^{M/2} C_{jp} e^{i\omega_p t}, \tag{61}$$

where

$$C_{j1} = \frac{1}{M}\hat{\varepsilon}_{j1}, \qquad C_{jp} = \frac{2}{M}\hat{\varepsilon}_{jp}, \qquad \omega_p = 2\pi\frac{p-1}{M\Delta t}. \tag{62}$$

So, the ratio of the axial to the transverse strain, obtained from measurements, is

$$\left(\frac{\varepsilon_z}{\varepsilon_y}\right)_{experimental} = \frac{C_{z1} + \sum_{p=2}^{M/2} C_{zp} e^{i\omega_p t}}{C_{y1} + \sum_{p=2}^{M/2} C_{yp} e^{i\omega_p t}}. \tag{63}$$

If the theoretical and experimental ratios in equations (58) and (63) should be equal at an arbitrary instant of time, it should be true for the constant parts that

$$-\frac{1}{\nu} = \frac{C_{z1}}{C_{y1}}, \tag{64}$$

and for every component $p$ of the Fourier series that

$$\frac{D_{zp}}{D_{yp}} = \frac{C_{zp}}{C_{yp}}, \tag{65}$$

where

$$D_{zp} = \mathbf{p}_z^{\mathrm{T}}\mathbf{q}_p, \qquad D_{yp} = \mathbf{p}_y^{\mathrm{T}}\mathbf{q}_p. \tag{66}$$

Adjusting $\nu$ to get the best fit between the theoretical and experimental ratios as a function of $\omega/\omega_0$, will give an estimation of $\nu$.

## 8. ESTIMATION OF COMPLEX AMPLITUDES FROM REDUNDANT STRAIN MEASUREMENTS

In a SHPB, the strains $\gamma_{yz}$ and $\gamma_{zx}$ are of less importance, at least, they are not directly measured. Therefore, the attention is here focused on the vector $\boldsymbol{\varepsilon}^a = [\varepsilon_x, \varepsilon_y, \varepsilon_z, \gamma_{xy}]^{\mathrm{T}}$ as given by equation (56). The theoretical expression for a strain component $\varepsilon_\beta(t)$, where $\beta$ is

one of $x$, $y$ and $z$, at position $(x_j, y_j, z_j)$ is then

$$\varepsilon_\beta(x_j, y_j, z_j, t) = \varepsilon_{j,theoretical}(t) = \mathbf{p}_j^T \boldsymbol{\varepsilon}^a, \tag{67}$$

where $\mathbf{p}_j$ is a vector, used to pick the strain component $\varepsilon_\beta$. Substitution of equation (56) into this relation gives

$$\varepsilon_{j,theoretical}(t) = \varepsilon_0 \mathbf{p}_j^T [-v, -v, 1, 0]^{\mathrm{T}} + \mathbf{p}_j^{\mathrm{T}} \sum_{p=2}^{M/2} \mathbf{q}_p(x_j, y_j)(A_p e^{-ik_p z_j} + B_p e^{ik_p z_j})\, e^{i\omega_p t}. \tag{68}$$

From measurements of the same strain component, and use of equation (61), one obtains

$$\varepsilon_{j,experimental}(t) = C_{j1} + \sum_{p=2}^{M/2} C_{jp} e^{i\omega_p t}. \tag{69}$$

The requirement that these expressions for the strain should be identical gives

$$\varepsilon_0 \mathbf{p}_j^{\mathrm{T}} [-v, -v, 1, 0]^{\mathrm{T}} = C_{j1} \tag{70}$$

for the first term and

$$\mathbf{p}_j^{\mathrm{T}} \mathbf{q}_p(x_j, y_j)(A_p e^{-ik_p z_j} + B_p e^{ik_p z_j}) = C_{jp} \tag{71}$$

for each component in the series. It can be seen that the two parameters $u_0$ and $v_0$ in equation (36), which represents rigid-body motion, cannot be determined from the strain measurements. Instead, these two parameters can be determined from the condition that the bar is quiescent at the beginning of the experiment. It can also be seen that the two unknowns $A_p$ and $B_p$ cannot be determined from a single equation (71).

Measurements made simultaneously at two or more, say $N$, positions lead to the systems of equations

$$\begin{bmatrix} \mathbf{p}_1^{\mathrm{T}} \\ \mathbf{p}_2^{\mathrm{T}} \\ \vdots \\ \mathbf{p}_N^{\mathrm{T}} \end{bmatrix} \begin{bmatrix} -v \\ -v \\ 1 \\ 0 \end{bmatrix} \varepsilon_0 = \begin{bmatrix} C_{11} \\ C_{21} \\ \vdots \\ C_{N1} \end{bmatrix} \tag{72}$$

and for each $p$,

$$\begin{bmatrix} e^{-ik_p z_1} & e^{ik_p z_1} \\ e^{-ik_p z_2} & e^{ik_p z_2} \\ \vdots & \vdots \\ e^{-ik_p z_N} & e^{ik_p z_N} \end{bmatrix} \begin{bmatrix} A_p \\ B_p \end{bmatrix} = \begin{bmatrix} C_{1p}/D_{1p} \\ C_{2p}/D_{2p} \\ \vdots \\ C_{Np}/D_{Np} \end{bmatrix}, \tag{73}$$

where

$$D_{jp} = \mathbf{p}_j^{\mathrm{T}} \mathbf{q}_p(x_j, y_j). \tag{74}$$

If $N > 1$ when estimating $\varepsilon_0$, and $N > 2$ when estimating $A_p$ and $B_p$, the systems of equations above are overdetermined, and can be solved by the least-squares method. An overdetermined system contains redundant information, and as a result, gives better accuracy when estimating $\varepsilon_0$, $A_p$ and $B_p$. If two rows in the system matrix in equation (73) are linearly dependent, some redundant information will be lost. This occurs if

$$k_p z_\alpha = k_p z_\beta + n\pi, \tag{75}$$

where $1 \leqslant \alpha, \beta \leqslant N$ and $n$ is an arbitrary integer. This relation will always be approximately satisfied for some $p$ if the frequency resolution is high. In terms of wavelength $\lambda (= 2\pi/k)$, this condition can be expressed as

$$z_\alpha - z_\beta \approx n \frac{\lambda_p}{2}. \tag{76}$$

If $N$ is a small number, or if the strain gauges are equidistant, i.e., $z_\alpha - z_\beta = z_\beta - z_\gamma = \cdots \approx n\lambda_p/2$, this may be a serious problem. One way to avoid the problem is to position one or more strain gauges where waves travelling in positive and negative direction, respectively, are separated in time. This means far enough from the end of a SHPB. One single measuring record can then be split into two measuring records, one for the wave travelling in positive $z$-direction, and one for the wave travelling in negative $z$-direction. The remaining parts of the records should be padded with zeros before a Fourier transform is made. After Fourier transformation, the two measuring records will give two constants $C^+$ and $C^-$ in equation (73). One row in the system of equations can then be separated into two rows,

$$\begin{bmatrix} e^{-ik_p z_\alpha} & 0 \\ 0 & e^{ik_p z_\alpha} \end{bmatrix} \begin{bmatrix} A_p \\ B_p \end{bmatrix} = \begin{bmatrix} C^+_{\alpha p}/D_{\alpha p} \\ C^-_{\alpha p}/D_{\alpha p} \end{bmatrix}, \tag{77}$$

which are clearly independent of each other.

It should be noted here that this separation should be done after $\varepsilon_0$ is estimated, since the constant strain is not associated to a direction. Another note is that the complete waves travelling in the two directions, or at least the major part, should have passed all measuring positions in the experiment.

## 9. EXPERIMENTS

A magnesium (alloy AZ61-F) bar with square cross-section was used. The side length of the cross-section was 12 mm ($a = 6$ mm), and the length of the bar was 2·37 m. The density was 1800 kg/m$^3$. Strain gauges measuring axial strain were placed at 1000, 750, 330 and 150 mm from one bar end. These positions are labelled 1–4, respectively. Two strain gauges on opposite sides of the bar were placed at each position and connected to opposite branches of Wheatstone bridges in order to cancel the effects of flexural waves. In addition, strain gauges measuring transverse strains were placed at position 1. The signals from the strain gauges were amplified and then recorded by a transient recorder (Nicolet Integra 20) with sampling frequency 1 MHz.

A projectile consisting of a 500 mm long bar with a circular cross-section with diameter 12 mm, manufactured in the same material as the square bar, was used to create longitudinal waves in the bar. The projectile was fired from an air gun.

Two experiments were carried out. The first was made to calibrate the bar. Axial and transverse strains in position 1 were recorded. The second experiment was carried out to estimate the mean displacements and stresses at the free end of the bar. Also, the energy flux through the bar end was calculated. Axial strains were measured at the four strain gauge positions in one single experiment. The first two positions were far enough from the bar end to enable separation in time of the incident and reflected waves. The data from the four strain gauge positions were used in six different ways in order to investigate the influence on the results from (a) the number of measuring positions used, and (b) if the incident and reflected waves were separated or not, in the data processing. The six cases were configured according to Table 1, where "S" means separated. "N" means not separated and "—" means not used.

TABLE 1

*Used measuring positions in data processing*

| Case | Pos. 1 | Pos. 2 | Pos. 3 | Pos. 4 |
|---|---|---|---|---|
| A | — | S | — | — |
| B | — | N | — | N |
| C | — | S | — | N |
| D | — | N | N | N |
| E | N | N | N | N |
| F | S | S | N | N |

## 10. RESULTS

The co-ordinate functions given in Appendix A were used in the computations. Explicit expressions for the matrices can be found in Appendix B. The parameter $n$, associated with the maximal order of the polynomial co-ordinate functions in the matrix $\mathbf{\Phi}$, was set to $n = 6$. No difference in the results was found with $n = 4$.

The results were normalized. The typical axial strain $\varepsilon_{ref} = 1{\cdot}82 \times 10^{-3}$ and duration $t_{ref} = 0{\cdot}2 \times 10^{-3}$ s of the incident wave were used to determine the reference quantities

$$u_{ref} = c_0 \varepsilon_{ref} t_{ref}, \tag{78}$$

$$\sigma_{ref} = E\varepsilon_{ref} \tag{79}$$

and

$$P_{ref} = 4a^2 E c_0 \varepsilon_{ref}^2. \tag{80}$$

### 10.1. EXPERIMENT 1: CALIBRATION

The measured strains versus time can be seen in Figure 1. The transverse strain has an offset of 0·2 in order to separate the signals. From the time difference between the front of the incident and reflected waves, Young's modulus $E$ was determined to be 45 GPa.

The complex-valued amplitudes $C_{zp}$ and $C_{yp}$ in equation (65) were obtained from a DFT of the strains in Figure 1. The ratio $C_{zp}/C_{yp}$ will have large errors if the denominator is close to zero, which will occur if the energy content in the frequency component is low. The energy content is related to the square of the amplitude, cf. the last term in equation (54), which makes the quantity $|C_{yp}^2|$ a good measure of which components to be accepted to use in the calibrating procedure. Figure 2 shows this quantity versus dimensionless angular frequency. The lower limit for acceptance of the components is shown as the smooth curve in the figure. The limit function is constructed to accept the frequency components with high energy content compared to its neighbouring frequencies.

Figure 3 shows the absolute values of the ratios of amplitudes for axial and transverse strains versus angular frequency. The solid line is obtained from the theoretical model ($D_z/D_y$) and the crosses come from the measurements ($C_z/C_y$). The experimental values at low frequencies are the most reliable as these frequencies are associated with the highest energy, cf. Figure 2. At $\omega/\omega_0 = 0$, the value should theoretically be $1/\nu$. From these experiments, $\nu$ was estimated to be 0·3021, which was used when calculating $D_z/D_y$ in the figure.

Figure 4 shows the phase angle of the same complex-valued ratios as in Figure 3. It can be seen that for $\omega/\omega_0 > 1{\cdot}4$, the data are not reliable. This frequency corresponds to the

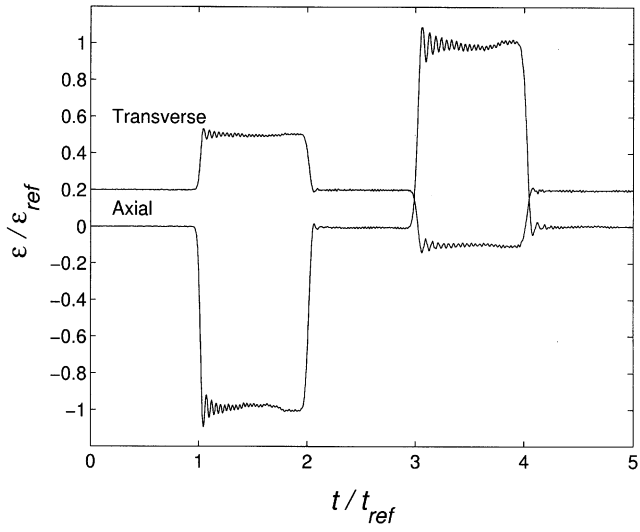


Figure 1. Measured axial and transverse normalized strains at position 1 versus normalized time. Transverse strain has offset 0·2 for clarity.

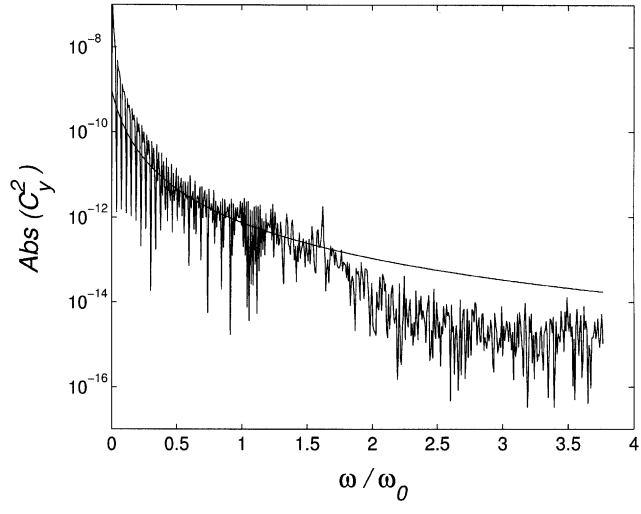


Figure 2. Absolute value of squared complex amplitudes for measured transverse strains at position 1 versus dimensionless angular frequency. Lower limit for accepted values in calibrating procedure is marked by the smooth curve.

wavelength $\lambda = 4a$ (two side lengths of the bar). In Experiment 2, frequencies higher than $\omega/\omega_0 = 1{\cdot}4$ were filtered.

## 10.2. EXPERIMENT 2: END CONDITIONS AND ENERGY FLUX

The strains at the four strain gauge positions versus time is shown in Figure 5. The strains have offsets which separate them in the figure. It can be seen that the incident and

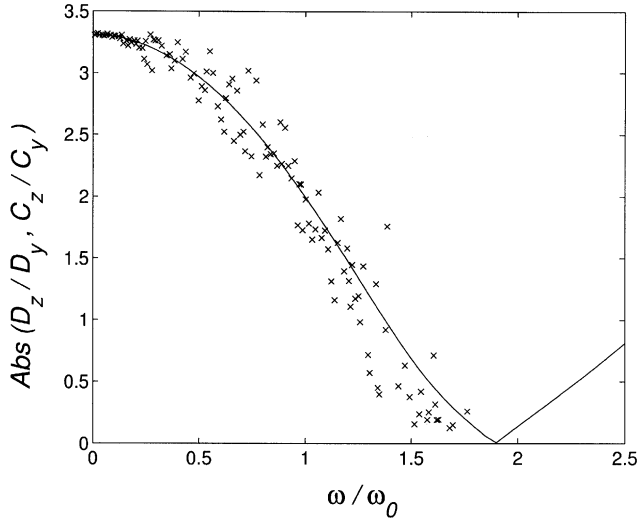


Figure 3. Absolute value of ratio of complex amplitudes for axial and transverse strains versus dimensionless angular frequency from theoretical model (solid line) and measurements (crosses).

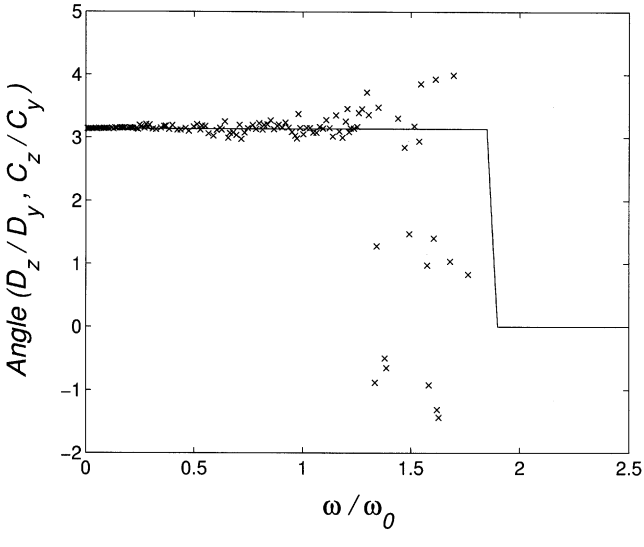


Figure 4. Phase angle of ratio of complex amplitudes for axial and transverse strains versus dimensionless angular frequency for theoretical model (solid line) and measurements (crosses).

reflected waves are separated in time at the first two strain gauge positions, but not at the other two.

Figure 6 shows the mean axial displacements versus time at the bar end evaluated according to the six cases given in Table 1. Cases B–F have offsets for clarity.

Figure 7 shows the mean axial stress at the bar end versus time evaluated according to the six cases. As the bar end is free, the stresses should be zero. As mentioned earlier, the stress is normalized to the typical axial stress in the incident wave.

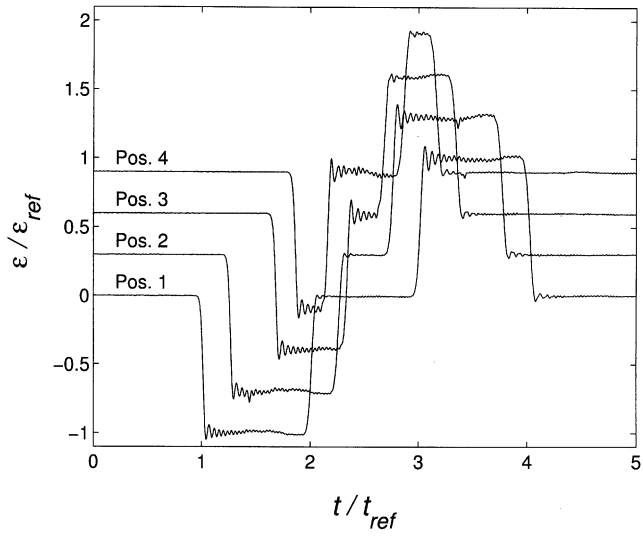


Figure 5. Normalized strains in the four measuring positions versus normalized time. Positions 2–4 have offsets 0·3, 0·6 and 0·9 for clarity.

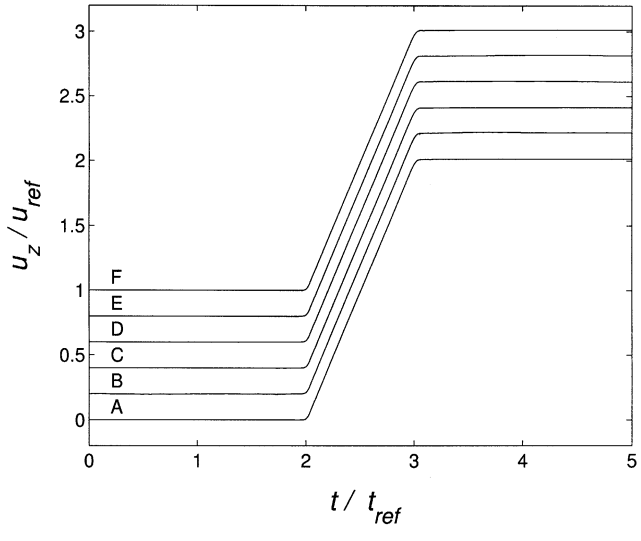


Figure 6. Normalized mean axial displacement over bar end versus normalized time for the six cases. Cases B–F have offsets 0·2, 0·4, ... , 1·0 for clarity.

Figure 8 shows energy flux through the bar end. The energy flux through a free bar end should be zero, and, again, the normalization is made with reference to the incident wave.

## 11. DISCUSSION

A mathematical model used to find dispersion relations, etc., for elastic stress waves in bars, and a method to solve the eigenvalue problem obtained, has been presented. The

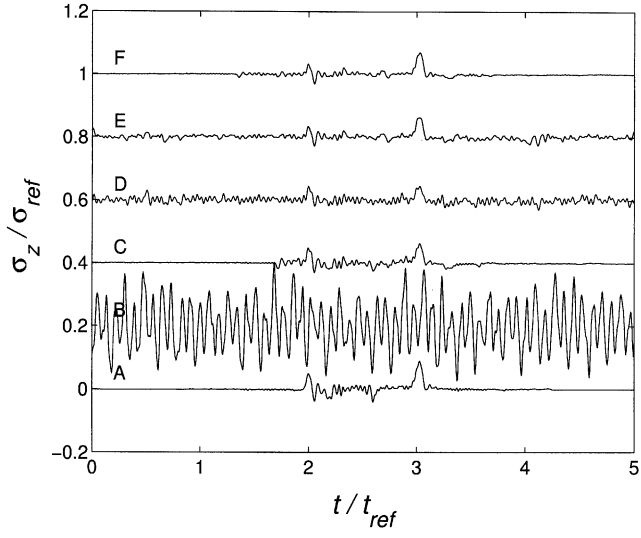


Figure 7. Normalized mean axial stress over bar end versus normalized time for the six cases. Cases B–F have offsets 0·2, 0·4, . . . , 1·0 for clarity.

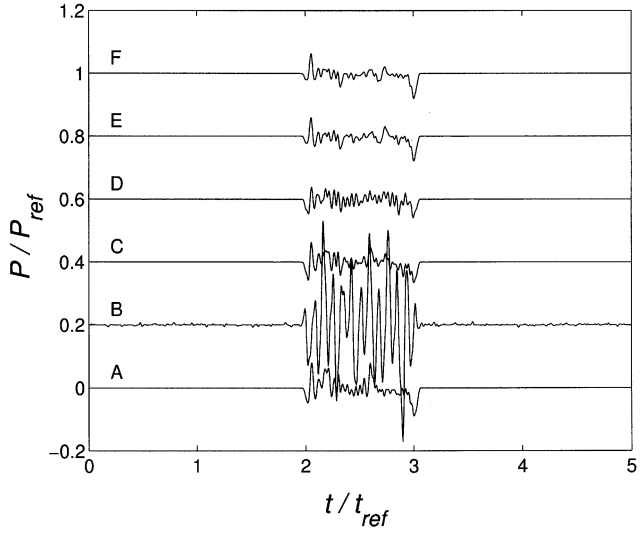


Figure 8. Normalized energy flux at bar end versus normalized time for the six cases. Cases B–F have offsets 0·2, 0·4, . . . , 1·0 for clarity.

model has been coupled to experimental data and used to evaluate wave propagation in the bar.

Information from the model has also been used to calibrate material data of the bar. By measuring both axial and transverse strains, the Poisson ratio $v$ can be accurately estimated. This procedure also gives information about the upper frequency limit for reliable data.

A method based on redundant measurements, used to increase the accuracy of the results, has also been developed. A possibility to increase the degree of redundancy prevails if the waves travelling in the two directions in the bar can be separated in time at a measuring position. One data record can then be split into two. The results show that the separation of waves improves the accuracy of the results significantly, e.g., cf. Figure 7 where cases A, C and F uses separation of waves. If such a separation is not possible, the number of measuring positions may have to be increased instead in order to get good results. Using only two measuring positions without any splitting of the data records appeared to give bad estimation for the stresses and energy flux in the bar. Again, cf. Figures 7 and 8 where case B uses this method. It can be seen that cases D and E, using more measuring positions but still no separation, gives better results. For estimation of the axial displacement at the end of the bar, cf. Figure 6 the same result was obtained for all cases. This is due to the fact that displacements are integrated from the measured strains, and the integration cancels small fluctuations.

## ACKNOWLEDGMENTS

The author expresses his appreciation of financial support from the Foundation for Knowledge and Competence Development, the National Graduate School of Scientific Computing and Metso Paper AB.

## REFERENCES

1. P. S. Follansbee and C. Frantz 1983 *Journal of Engineering Materials and Technology* **105**, 61–66. Wave propagation in the split Hopkinson pressure bar.
2. J. C. Gong, L. E. Malvern and D. A. Jenkins 1990 *Journal of Engineering Materials and Technology* **112**, 309–314. Dispersion investigation in the split Hopkinson pressure bar.
3. Z. Li and J. Lambros 1999 *Composites Science and Technology* **59**, 1097–1107. Determination of the dynamic response of brittle composites by the use of the split Hopkinson pressure bar.
4. A. Tyas and A. J. Watson 2000 *Experimental Mechanics* **40**, 331–337. Experimental evidence of Pochammer–Chree strain variations in elastic cylinders.
5. A. Tyas and A. J. Watson 2001 *International Journal of Impact Engineering* **25**, 87–101. An investigation of frequency domain dispersion correction of pressure bar signals.
6. L. Pochammer 1876 *Journal Für die reine und angewandte mathematik* **81**, 324–336. Ueber die fortpflanzungsgeschwindigkeiten kleiner schwingungen in einem unbegrentzen isotropen kreiszylinder.
7. C. Chree 1889 *Transactions of the Cambridge Philosophical Society* **14**, 250–369. The equations of an isotropic elastic solid in polar and cylindrical co-ordinates.
8. A.-C. Hladky-Hennion 1996 *Journal of Sound and Vibration* **194**, 119–136. Finite element analysis of the propagation of acoustic waves in waveguides.
9. V. V. Volovoi, D. H. Hodges, V. L. Berdichevsky and V. G. Sutyrin 1998 *Journal of Sound and Vibration* **215**, 1101–1120. Dynamic dispersion curves for non-homogeneous, anisotropic beams with cross-sections of arbitrary geometry.
10. H. Taweel, S. B. Dong and M. Kazic 2000 *International Journal of Solids and Structures* **37**, 1701–1726. Wave reflection from the free end of a cylinder with an arbitrary cross-section.
11. B. Lundberg and A. Henchoz 1977 *Experimental Mechanics* **17**, 216–218. Analysis of elastic waves from two-point strain measurement.
12. H. Zhao and G. Gary 1997 *Journal of the Mechanics and Physics of Solids* **45**, 1185–1202. A new method for the separation of wave. Application to the SHPB technique for an unlimited duration of measurement.
13. C. Bacon 1999 *International Journal of Impact Engineering* **22**, 55–69. Separation of waves propagating in an elastic or viscoelastic Hopkinson pressure bar with three-dimensional effects.
14. S. W. Park and M. Zhou 1999 *Experimental Mechanics* **39**, 287–294. Separation of elastic waves in split Hopkinson bars using one-point strain measurements.

15. L. Hillström, M. Mossberg and B. Lundberg 2000 *Journal of Sound and Vibration* **230**, 689–707. Identification of complex modulus from measured strains in an axially impacted bar using least squares.
16. S. Widehammar, P. A. Gradin and B. Lundberg 2001 *Journal of Sound and Vibration* **246**, 853–876. Approximate determination of dispersion relations and displacement fields associated with elastic waves in bars, method based on matrix formulation of Hamilton's principle.
17. M. M. Al-Mousawi, S. R. Reid and W. F. Deans 1997 *Proceedings of the Institution of Mechanical Engineers* **211**, 273–292. The use of split Hopkinson pressure bar techniques in high strain rate materials testing.
18. L. Lagerkvist and B. Lundberg 1982 *Journal of Sound and Vibration* **80**, 389–399. Mechanical impedance gauge based on measurement of strains on a vibrating rod.
19. J. Carlsson, K. G. Sundin and B. Lundberg 1990 *International Journal of Rock Mechanics and mining Sciences and Geomechanics Abstracts* **27**, 553–558. A method for determination of in-hole dynamic force-penetration data from two-point strain measurement on a percussive drill rod.
20. K. G. Sundin and B. O. Åhrström 1999 *Journal of Sound and Vibration* **222**, 669–677. Method for investigation of frictional properties at impact loading.
21. H. Kolsky 1963 *Stress Waves in Solids* New York: Dover Publications.
22. A. Ruhe 1973 *SIAM Journal of Numerical Analysis* **10**, 674–689. Algorithms for the nonlinear eigenvalue problem.

## APPENDIX A: CO-ORDINATE FUNCTIONS FOR LONGITUDINAL WAVES IN A BAR WITH SQUARE CROSS-SECTION

Longitudinal waves have the following symmetry conditions:

$$u_x(x,y) = u_x(x,-y) = -u_x(-x,y), \qquad u_y(x,y) = u_x(y,x) \tag{A.1, A.2}$$

and

$$u_z(x,y) = u_z(x,-y) = u_z(-x,y) = u_z(y,x). \tag{A.3}$$

The matrix of co-ordinate functions is

$$\underset{3\times m}{\boldsymbol{\Phi}} = \begin{bmatrix} \boldsymbol{\Phi}^a & \mathbf{0} \\ \mathbf{0} & \boldsymbol{\Phi}^b \end{bmatrix}, \tag{A.4}$$

where $(3 \times m)$ is the size of the matrix and

$$m = m_a + m_b. \tag{A.5}$$

The submatrices are

$$\underset{2\times m_a}{\boldsymbol{\Phi}^a} = \begin{bmatrix} \boldsymbol{\phi}_x^{\mathrm{T}} \\ \boldsymbol{\phi}_y^{\mathrm{T}} \end{bmatrix}, \qquad \underset{1\times m_b}{\boldsymbol{\Phi}^b} = \boldsymbol{\phi}_z^{\mathrm{T}}, \tag{A.6}$$

where

$$\boldsymbol{\phi}_x^{\mathrm{T}} = \left[\boldsymbol{\phi}_{x0}^{\mathrm{T}}\, \boldsymbol{\phi}_{x2}^{\mathrm{T}}\, \boldsymbol{\phi}_{x4}^{\mathrm{T}} \ldots \boldsymbol{\phi}_{xn}^{\mathrm{T}}\right], \qquad \boldsymbol{\phi}_z^{\mathrm{T}} = \left[\boldsymbol{\phi}_{z0}^{\mathrm{T}}\, \boldsymbol{\phi}_{z2}^{\mathrm{T}}\, \boldsymbol{\phi}_{z4}^{\mathrm{T}} \ldots \boldsymbol{\phi}_{zn}^{\mathrm{T}}\right] \tag{A.7, A.8}$$

and

$$\boldsymbol{\phi}_y(x,y) = \boldsymbol{\phi}_x(y,x). \tag{A.9}$$

The vectors $\boldsymbol{\phi}_x$ and $\boldsymbol{\phi}_y$ have the length

$$m_a = \left(\frac{n}{2} + 1\right)^2 \tag{A.10}$$

and the vector $\boldsymbol{\phi}_z$ has the length

$$m_b = \frac{1}{2}\left(\frac{n}{2}+1\right)\left(\frac{n}{2}+2\right). \tag{A.11}$$

The subvectors are

$$\boldsymbol{\phi}_{xk}^{\mathrm{T}} = \left(\frac{x}{a}\right)^{k+1}\boldsymbol{\varphi}_n^{\mathrm{T}}(y), \qquad \boldsymbol{\phi}_{zk}^{\mathrm{T}} = \left(\frac{x}{a}\right)^{k}\boldsymbol{\varphi}_k^{\mathrm{T}}(y) + \left(\frac{y}{a}\right)^{k}\boldsymbol{\varphi}_k^{\mathrm{T}}(x), \tag{A.12, A.13}$$

where the $\boldsymbol{\varphi}$-vectors are defined by

$$\boldsymbol{\varphi}_k^{\mathrm{T}}(x) = \left[1 \left(\frac{x}{a}\right)^2 \left(\frac{x}{a}\right)^4 \ \ldots \ \left(\frac{x}{a}\right)^k\right]. \tag{A.14}$$

The parameter $n$ is chosen according to wanted order on the polynomial co-ordinate functions. The value $(n+1)$ is the maximal order for variables $x$ and $y$, and $n$ is the maximal order for $z$.

## APPENDIX B: INTEGRATED MATRICES

In the following formulas, the parameters $n$, $m$, $m_a$ and $m_b$ are defined in Appendix A, and the parameters $\alpha_1$, $\alpha_2$ and $\alpha_3$ are the elastic constants from equation (21).

### B.1. MATRICES $\mathbf{K}_0$ AND $\tilde{\mathbf{K}}_0$

$$\underset{m\times m}{\mathbf{K}_0} = \underset{m\times m}{\tilde{\mathbf{K}}_{\mathbf{0}}} = \begin{bmatrix} \mathbf{K}_{0a} & \mathbf{0} \\ \mathbf{0} & \mathbf{K}_{0b} \end{bmatrix}, \qquad \underset{m_a\times m_a}{\mathbf{K}_{0a}} = \begin{bmatrix} \mathbf{K}_{0a}^{00} & \mathbf{K}_{0a}^{02} & \cdots & \mathbf{K}_{0a}^{0n} \\ \mathbf{K}_{0a}^{20} & \mathbf{K}_{0a}^{22} & \cdots & \mathbf{K}_{0a}^{2n} \\ \vdots & \vdots & \ddots & \vdots \\ \mathbf{K}_{0a}^{n0} & \mathbf{K}_{0a}^{n2} & \cdots & \mathbf{K}_{0a}^{nn} \end{bmatrix}, \tag{B.1, B.2}$$

$$\underset{m_b\times m_b}{\mathbf{K}_{0b}} = \begin{bmatrix} \mathbf{K}_{0b}^{00} & \mathbf{K}_{0b}^{02} & \cdots & \mathbf{K}_{0b}^{0n} \\ \mathbf{K}_{0b}^{20} & \mathbf{K}_{0b}^{22} & \cdots & \mathbf{K}_{0b}^{2n} \\ \vdots & \vdots & \ddots & \vdots \\ \mathbf{K}_{0b}^{n0} & \mathbf{K}_{0b}^{n2} & \cdots & \mathbf{K}_{0b}^{nn} \end{bmatrix}, \tag{B.3}$$

$$\underset{(n/2+1)\times(n/2+1)}{\mathbf{K}_{0a}^{kl}} = \begin{bmatrix} K_{0a}^{kl00} & K_{0a}^{kl02} & \cdots & K_{0a}^{kl0n} \\ K_{0a}^{kl20} & K_{0a}^{kl22} & \cdots & K_{0a}^{kl2n} \\ \vdots & \vdots & \ddots & \vdots \\ K_{0a}^{kln0} & K_{0a}^{kln2} & \cdots & K_{0a}^{klnn} \end{bmatrix}, \tag{B.4}$$

$$\underset{(k/2+1)\times(l/2+1)}{\mathbf{K}_{0b}^{kl}} = \begin{bmatrix} K_{0b}^{kl00} & K_{0b}^{kl02} & \cdots & K_{0b}^{kl0l} \\ K_{0b}^{kl20} & K_{0b}^{kl22} & \cdots & K_{0b}^{kl2l} \\ \vdots & \vdots & \ddots & \vdots \\ K_{0b}^{klk0} & K_{0b}^{klk2} & \cdots & K_{0b}^{klkl} \end{bmatrix}, \tag{B.5}$$

$$K_{0a}^{klpq} = 8\alpha_1 \frac{(k+1)(l+1)}{(k+l+1)(p+q+1)} + 8\alpha_2 \frac{(k+1)(l+1)}{(k+q+1)(l+p+1)}$$

$$+ 8\alpha_3 \left( \frac{pq}{(k+l+3)(p+q-1)} + \frac{pq}{(k+q+1)(l+p+1)} \right), \tag{B.6}$$

$$K_{0b}^{klpq} = 8\alpha_3 \left( \frac{kl}{(k+l-1)(p+q+1)} + \frac{kq}{(k+q-1)(l+p+1)} \right.$$

$$\left. + \frac{lp}{(l+p-1)(k+q+1)} + \frac{pq}{(p+q+1)(k+l+1)} \right). \tag{B.7}$$

## B.2. MATRICES $\mathbf{K}_1$ AND $\tilde{\mathbf{K}}_1$

$$\underset{m\times m}{\mathbf{K}_1} = \begin{bmatrix} \mathbf{0} & \mathbf{K}_{1b} \\ \mathbf{K}_{1a} & \mathbf{0} \end{bmatrix}, \qquad \underset{m\times m}{\tilde{\mathbf{K}}_1} = \begin{bmatrix} \mathbf{0} & \mathbf{K}_{1b} \\ -\mathbf{K}_{1a} & \mathbf{0} \end{bmatrix}, \tag{B.8}$$

$$\underset{m_b\times m_a}{\mathbf{K}_{1a}} = \begin{bmatrix} \mathbf{K}_{1a}^{00} & \mathbf{K}_{1a}^{02} & \cdots & \mathbf{K}_{1a}^{0n} \\ \mathbf{K}_{1a}^{20} & \mathbf{K}_{1a}^{22} & \cdots & \mathbf{K}_{1a}^{2n} \\ \vdots & \vdots & \ddots & \vdots \\ \mathbf{K}_{1a}^{n0} & \mathbf{K}_{1a}^{n2} & \cdots & \mathbf{K}_{1a}^{nn} \end{bmatrix}, \qquad \underset{m_a\times m_b}{\mathbf{K}_{1b}} = \begin{bmatrix} \mathbf{K}_{1b}^{00} & \mathbf{K}_{1b}^{02} & \cdots & \mathbf{K}_{1b}^{0n} \\ \mathbf{K}_{1b}^{20} & \mathbf{K}_{1b}^{22} & \cdots & \mathbf{K}_{1b}^{2n} \\ \vdots & \vdots & \ddots & \vdots \\ \mathbf{K}_{1b}^{n0} & \mathbf{K}_{1b}^{n2} & \cdots & \mathbf{K}_{1b}^{nn} \end{bmatrix}, \tag{B.9, B10}$$

$$\underset{(k/2+1)\times(n/2+1)}{\mathbf{K}_{1a}^{kl}} = \begin{bmatrix} K_{1a}^{kl00} & K_{1a}^{kl02} & \cdots & K_{1a}^{kl0n} \\ K_{1a}^{kl20} & K_{1a}^{kl22} & \cdots & K_{1a}^{kl2n} \\ \vdots & \vdots & \ddots & \vdots \\ K_{1a}^{klk0} & K_{1a}^{klk2} & \cdots & K_{1a}^{klkn} \end{bmatrix}, \tag{B.11}$$

$$\underset{(n/2+1)\times(l/2+1)}{\mathbf{K}_{1b}^{kl}} = \begin{bmatrix} K_{1b}^{kl00} & K_{1b}^{kl02} & \cdots & K_{1b}^{kl0l} \\ K_{1b}^{kl20} & K_{1b}^{kl22} & \cdots & K_{1b}^{kl2l} \\ \vdots & \vdots & \ddots & \vdots \\ K_{1b}^{kln0} & K_{1b}^{kln2} & \cdots & K_{1b}^{klnl} \end{bmatrix}, \tag{B.12}$$

$$K_{1a}^{klpq} = 8\alpha_2 \left( \frac{l+1}{(k+l+1)(p+q+1)} + \frac{l+1}{(l+p+1)(k+q+1)} \right), \tag{B.13}$$

$$K_{1b}^{klpq} = 8\alpha_3 \left( \frac{l}{(k+l+1)(p+q+1)} + \frac{q}{(k+q+1)(l+p+1)} \right). \tag{B.14}$$

### B.3. MATRICES $\mathbf{K}_2$ AND $\tilde{\mathbf{K}}_2$

$$\underset{m\times m}{\mathbf{K}_2} = \underset{m\times m}{\tilde{\mathbf{K}}_2} = \begin{bmatrix} \mathbf{K}_{2a} & \mathbf{0} \\ \mathbf{0} & \mathbf{K}_{2b} \end{bmatrix}, \qquad \underset{m_a\times m_a}{\mathbf{K}_{2a}} = \begin{bmatrix} \mathbf{K}_{2a}^{00} & \mathbf{K}_{2a}^{02} & \cdots & \mathbf{K}_{2a}^{0n} \\ \mathbf{K}_{2a}^{20} & \mathbf{K}_{2a}^{22} & \cdots & \mathbf{K}_{2a}^{2n} \\ \vdots & \vdots & \ddots & \vdots \\ \mathbf{K}_{2a}^{n0} & \mathbf{K}_{2a}^{n2} & \cdots & \mathbf{K}_{2a}^{nn} \end{bmatrix}, \tag{B.15, B.16}$$

$$\underset{m_b\times m_b}{\mathbf{K}_{2b}} = \begin{bmatrix} \mathbf{K}_{2b}^{00} & \mathbf{K}_{2b}^{02} & \cdots & \mathbf{K}_{2b}^{0n} \\ \mathbf{K}_{2b}^{20} & \mathbf{K}_{2b}^{22} & \cdots & \mathbf{K}_{2b}^{2n} \\ \vdots & \vdots & \ddots & \vdots \\ \mathbf{K}_{2b}^{n0} & \mathbf{K}_{2b}^{n2} & \cdots & \mathbf{K}_{2b}^{nn} \end{bmatrix}, \tag{B.17}$$

$$\underset{(n/2+1)\times(n/2+1)}{\mathbf{K}_{2a}^{kl}} = \begin{bmatrix} K_{2a}^{kl00} & K_{2a}^{kl02} & \cdots & K_{2a}^{kl0n} \\ K_{2a}^{kl20} & K_{2a}^{kl22} & \cdots & K_{2a}^{kl2n} \\ \vdots & \vdots & \ddots & \vdots \\ K_{2a}^{kln0} & K_{2a}^{kln2} & \cdots & K_{2a}^{klnn} \end{bmatrix}, \tag{B.18}$$

$$\underset{(k/2+1)\times(l/2+1)}{\mathbf{K}_{2b}^{kl}} = \begin{bmatrix} K_{2b}^{kl00} & K_{2b}^{kl02} & \cdots & K_{2b}^{kl0l} \\ K_{2b}^{kl20} & K_{2b}^{kl22} & \cdots & K_{2b}^{kl2l} \\ \vdots & \vdots & \ddots & \vdots \\ K_{2b}^{klk0} & K_{2b}^{klk2} & \cdots & K_{2b}^{klkl} \end{bmatrix}, \tag{B.19}$$

$$K_{2a}^{klpq} = \frac{8\alpha_3}{(k+l+3)(p+q+1)}, \tag{B.20}$$

$$K_{2b}^{klpq} = 8\alpha_1\left(\frac{1}{(k+l+1)(p+q+1)} + \frac{1}{(k+q+1)(l+p+1)}\right). \tag{B.21}$$

### B.4. MATRICES $\mathbf{M}$ AND $\tilde{\mathbf{M}}$

The matrices $\mathbf{M}$ and $\tilde{\mathbf{M}}$ are same as $\mathbf{K}_2$, if the parameters $\alpha_1$ and $\alpha_3$ are set to 1 in equations (B.20) and (B.21).

### B.5. MATRIX $\mathbf{F}$

$$\underset{(2+1)\times(m_a+m_b)}{\mathbf{F}} = \begin{bmatrix} \mathbf{0} & \mathbf{0} \\ \mathbf{0} & \mathbf{f}_z^{\mathrm{T}} \end{bmatrix}, \qquad \mathbf{f}_z^{\mathrm{T}} = \left[\left(\mathbf{f}_z^0\right)^{\mathrm{T}} \left(\mathbf{f}_z^2\right)^{\mathrm{T}} \cdots \left(\mathbf{f}_z^n\right)^{\mathrm{T}}\right], \tag{B.22, B.23}$$

$$(\mathbf{f}_z^k)^{\mathrm{T}} = [f_z^{k0} f_z^{k2} \cdots f_z^{kk}], \qquad f_z^{kp} = \frac{2}{(k+1)(p+1)}. \tag{B.24, B.25}$$

## B.6. MATRIX $\mathbf{F}_{xy}$

$$\underset{6\times m}{\mathbf{F}_{xy}} = \frac{1}{a}\begin{bmatrix} \mathbf{F}_{xy}^a & \mathbf{0} \\ \mathbf{0} & \mathbf{0} \end{bmatrix}, \qquad \underset{4\times m_a}{\mathbf{F}_{xy}^a} = \begin{bmatrix} \mathbf{f}_{xy}^{\mathrm{T}} \\ \mathbf{f}_{xy}^{\mathrm{T}} \\ \mathbf{0} \\ \mathbf{0} \end{bmatrix}, \tag{B.26}$$

where $a$ is half the side length of the square cross-section.

$$\mathbf{f}_{xy}^{\mathrm{T}} = \left[\left(\mathbf{f}_{xy}^0\right)^{\mathrm{T}} \left(\mathbf{f}_{xy}^2\right)^{\mathrm{T}} \cdots \left(\mathbf{f}_{xy}^n\right)^{\mathrm{T}}\right], \qquad \left(\mathbf{f}_{xy}^k\right)^{\mathrm{T}} = \left[f_{xy}^{k0} \; f_{xy}^{k2} \; \cdots \; f_{xy}^{kn}\right], \tag{B.27, B.28}$$

$$f_{xy}^{kp} = \frac{1}{(p+1)}. \tag{B.29}$$